HIGH-RESISTIVITY SOFT MAGNETIC THIN FILMS USING CoFe METAL/NATIVE OXIDE MULTILAYERS (INVITED)

Geoffrey S. D. Beach
The University of Texas at Austin
Department of Physics
1 University Station C1600
Austin, TX 78712-1081

Ami E. Berkowitz and Fred T. Parker
University of California, San Diego
Center for Magnetic Recording Research 0401
9500 Gilman Drive
La Jolla, CA 92093-0401

David J. Smith
Arizona State University
Department of Physics and Astronomy and
Center for Solid State Science
Tempe, AZ 85287-1504

ABSTRACT

Magnetic thin films suitable for gigahertz operation must simultaneously achieve soft properties, high saturation magnetization, and a high resistivity. The recently-introduced metal/native oxide multilayer (MNOM) composite meets these requirements. This system consists of nanogranular high-moment Co_xFe_{100-x} layers separated by ultrathin *magnetic* native oxide layers that isolate the metallic layers electrically while, in contrast to nonmagnetic oxides, coupling them magnetically and augmenting the volume-averaged saturation magnetization. The MNOM system delivers high permeability with a bandwidth of several GHz for most of the Co_xFe_{100-x} alloy composition range. This paper will review the soft magnetic properties of the MNOM system and describe the magnetic properties of the *buried* native oxide layers.

INTRODUCTION

There is strong industrial demand for new high-permeability thin films with GHz operating frequencies. Applications include write poles and shields in magnetic recording heads, soft underlayers for perpendicular media, and integrated thin film inductor cores. One challenge to meeting this demand is the necessity of achieving a higher resistivity than conventional materials, to limit eddy current screening, while maintaining or exceeding the high permeability and saturation magnetization of those materials. Among the more successful approaches to the problem are granular metal/insulator composites, in which high-moment metallic nanoparticles o are embedded in a nonmagnetic insulating matrix, such as Al_2O_3 [1]-[3]. Although such films have demonstrated soft magnetic properties, large magnetizations, and high resistivities, there are important limitations to simultaneously optimizing these properties. Resistivity comes at the expense of the volume-averaged saturation magnetization, which decreases in proportion to increasing oxide fraction. Furthermore, soft magnetic properties are only obtained for metal volume fractions approaching metallic percolation, in order to allow interparticle "exchange averaging" to "smooth" local variations in anisotropy magnitude and direction.

A promising new approach [4], using Co_xFe_{100-x} metal/native oxide multilayers (MNOM) [shown schematically in Fig. 1(a)] aimed to replace the nonmagnetic oxide phase with a *magnetic* oxide. A magnetic oxide offers the possibility of isolating metallic regions electrically

while coupling them magnetically. In addition, a moment-bearing oxide detracts less from the net magnetization, permitting a higher magnetization for a given metallic fraction.

The Co_xFe_{100-x} MNOM system has demonstrated ideal soft magnetic properties [4], a large magnetization due in part to a significant contribution by the oxide [5], [6], and excellent high-frequency characteristics with bandwidths of several GHz [7]. This paper will review the technologically-significant soft magnetic properties and high-frequency characteristics of the MNOM system and discuss the magnetic properties of the buried native Co_xFe_{100-x} oxide layers. The oxide has a net moment comparable to the bulk ferrites, but its spin structure is significantly more complex. The magnetism of these ultrathin *buried* oxide layers, in which all spins are either directly or indirectly coordinated by metallic (Co)Fe, is *supported* by the metal and collapses in the absence of the metal.

FABRICATION, MICROSTRUCTURE, AND RESISTIVITY

The MNOM structure [see Fig. 1(a)], consists of alternating nanocrystalline Co_xFe_{100-x} metal and *native* oxide layers. The metal layers (typically a few nm) were dc sputter-deposited from stoichiometric Co_xFe_{100-x} alloy targets. Following deposition of each layer, the sputtering source was shuttered and the layer was exposed *in situ* to $\sim 8\times10^{-5}$ Torr of O_2 for 10 s. Each exposure was followed by a 60 s pause to allow the O_2 partial pressure to drop to its background level before deposition of the subsequent metal layer. The notation $[Co_xFe_{100-x}(t_0)/\text{oxide}]_N$ describes a MNOM with N metal/native oxide bilayers, each formed by oxidizing a Co_xFe_{100-x} metal layer of nominal thickness t_0. All depositions were performed in the presence of a dc magnetic field (~100 Oe), establishing a uniaxial anisotropy, and were capped with a 50-100 Å SiO_2 layer.

The cross-sectional transmission electron micrograph (TEM) of Fig. 1(b) shows the microstructure of a $[Co_{50}Fe_{50}(20\ Å)/\text{oxide}]_{50}$ film. The layers are nanocrystalline with lateral grain sizes on the order of a few nm. The metal and oxide are distinguished by dark and light contrast, respectively. Lattice fringes are visible in both metal and oxide and span several layers in some regions, indicating locally-epitaxial metal/oxide and oxide/metal growth. In other regions, the oxide layers appear to disrupt the metallic grain growth.

The oxide layer thickness is passivation-limited [8], and is very reproducible, independent of t_0. Mössbauer and EXAFS studies of this system [5] find ~8.4 Å of metal to oxidize in each layer for the pure Fe MNOM system, while somewhat less metal oxidizes under the same conditions for Co_xFe_{100-x}-based films (~7.1 Å for $x = 50$ and ~6.3 Å for $x = 90$).

The in-plane resistivity ρ of MNOM films is substantially larger than for bulk Co_xFe_{100-x}. As t_0 decreases from 20 Å to 10 Å, ρ increases from ~120 to ~600 $\mu\Omega$-cm for $Co_{50}Fe_{50}$-based films [Fig. 1(c)] and reaches 12 mΩ-cm for Fe-based MNOMs. For thicker t_0, the metal layers are percolated in the plane, evidenced metallic $\rho(T)$, but as t_0 is reduced below ~16 Å, the conductivity becomes thermally activated, as seen in the inset of Fig. 1(c) for $Co_{50}Fe_{50}$ MNOMs.

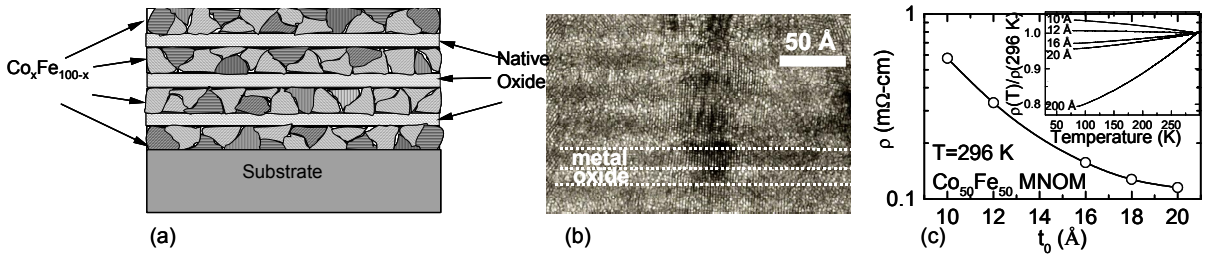

Fig. 1. (a) Schematic of the metal/native oxide multilayer structure. (b) High resolution transmission electron micrograph of $[Co_{50}Fe_{50}(20\ Å)/\text{oxide}]_{50}$. (c) In-plane room-temperature resistivity and (inset) its normalized temperature dependence for $[Co_{50}Fe_{50}(t_0)/\text{oxide}]_N$ films.

Similar $\rho(T)$ characteristics exist for Fe MNOMs,, and TEM studies show an increase in layer granularity and discontinuity coinciding with the onset of thermally-activated conductivity. The layer morphology can be varied from continuous to discontinuous through the layer thickness t_0.

SOFT MAGNETIC PROPERTIES OF THE COMPOSITE

Quasistatic Magnetic Characteristics

MNOM films, when compared to continuous films of the same alloy composition, exhibit three distinguishing magnetic characteristics: a substantial reduction in coercivity, an extremely low-dispersion in-plane uniaxial anisotropy, and only a modest decrease in volume-averaged saturation magnetization because of a significant contribution to the net moment by the native oxide [4], [5]. This section will focus on the magnetic properties and their variation with alloy composition for a series of MNOM films with $t_0 = 20$ Å.

Fig. 2(a) shows the in-plane easy-axis hysteresis loop of a $[Co_{50}Fe_{50}(20\ Å)/oxide]_{10}$ MNOM and that of a continuous 200 Å $Co_{50}Fe_{50}$ film. Compared to the continuous film, the coercivity (H_c) of the MNOM film is reduced tenfold and the loop squareness is significantly enhanced. The high remanent magnetization ratio of the MNOM, $M_r / M_s > 0.995$, is maintained until just prior to switching, which occurs abruptly over a field range of less than 1 Oe.

The hysteresis loops of the continuous $Co_{50}Fe_{50}$(200 Å) film are nearly isotropic in the plane with a coercivity of ~100 Oe, despite the presence of an in-plane alignment field during deposition. By contrast, the MNOM film shows a strong, in-plane uniaxial anisotropy, seen in the hysteresis loops of Fig. 2(b) measured parallel and perpendicular to the deposition field-induced easy axis. Particularly striking is the ideally closed and linear hard axis loop, indicating extremely low anisotropy dispersion. Such a lossless, linear magnetic response would be particularly beneficial to applications in magnetic recording and telecommunications.

The soft magnetic properties observed for $[Co_{50}Fe_{50}(20\ Å)/oxide]_N$ are representative of the MNOM system throughout much of the Co_xFe_{100-x} composition range. Several parameters characterizing these properties are plotted in Figs. 2(c)-(d) versus x. For pure Co, the system is *not* soft, with a coercivity H_c of ~230 Oe and ~160 Oe along the nominal easy and hard axes, respectively. However, a crossover to soft magnetic properties occurs near $x = 90$, where the hard-axis H_c falls close to zero and the easy axis loops become extremely square. The easy-axis

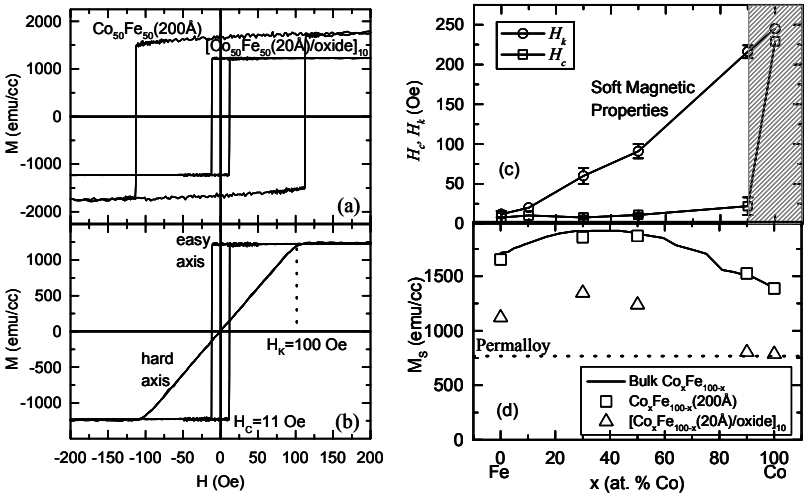

Fig. 2. (a) In-plane hysteresis loops for a $[Co_{50}Fe_{50}(20\ Å)/oxide]_{10}$ MNOM and a continuous $Co_{50}Fe_{50}$ film of the same total CoFe thickness. (b) In-plane easy and hard axis loops for the $[Co_{50}Fe_{50}(20\ Å)/oxide]_{10}$ MNOM. Magnetization is normalized to the total sample volume (including expansion due to oxidation in the MNOM) (c) Variation of coercivity and anisotropy field with composition for $[Co_xFe_{100-x}(20\ Å)/oxide]_{10}$ MNOM films of varying x. (d) Saturation magnetization of Co_xFe_{100-x} MNOM films, compared to bulk Co_xFe_{100-x}.

H_c of ~33 Oe for x = 90, drops to a composition-independent value of ~8-12 Oe for $x \leq 50$, while the hard-axis H_c remains ≤ 1.5 Oe for all compositions from 0 to 90. The low-dispersion uniaxial anisotropy present for all of these compositions has a magnitude H_k that increases almost linearly with Co fraction [Fig. 2(c)], from ~10 Oe for x = 0 to ~220 Oe for x = 90.

Figure 2(d) shows that the volume-averaged saturation magnetization M_s for $[Co_xFe_{100-x}$(20 Å)/oxide$]_N$ MNOM films is large, reaching 1350 emu/cc at x = 30, despite the oxidation of a significant quantity of the metal [5]. The results are compared with M_s of bulk Co_xFe_{100-x} and of 200 Å continuous films. M_s of the MNOMs exceeds that of Permalloy for all x, and is larger than can be accounted for by the metal alone, given the fraction of metal that remains unoxidized [5]. It is shown below that the native oxide contributes significantly to this magnetization.

High Frequency Magnetic Response

These quasistatic magnetic properties suggest favorable high-frequency characteristics. The measured H_k and M_s predict a permeability ($\mu_{dc} = B_s/H_k$) ranging from 50 to 1400 and resonance frequency ($f_{FMR} = \gamma\sqrt{M_s H_k}$ for simple uniform precession) ranging from 1.3 to 5.6 GHz, depending on alloy composition x. The "tunability" of μ_{dc} and f_{FMR} through H_k, which is a linear in x, provides an advantageous method to tailor the MNOM response to a particular application. However, given its complex two-phase microstructure, the response need not be single-mode uniform precession, and effects such as inhomogeneous line broadening or oxide relaxation could conceivably degrade the high-frequency performance.

The dynamical magnetic response of several $[Co_xFe_{100-x}$(20 Å)/oxide$]_{50}$ MNOM films, measured using pulsed inductive microwave magnetometry (PIMM) [9] was reported in [7], as summarized in Table I. The dynamic response *was* reasonably well-described by underdamped single-mode uniform precession, with intrinsic precessional frequencies (f_p) close to those predicted (f_{FMR}) based on the quasistatic M_s and H_k. The effective "dynamical" H_k, determined by fitting the bias-field dependence of f_p to the Kittel equation, was consistent with the value taken from quasistatic measurements. The damping values (α) were low, and, along with the high precessional frequencies, offer promise for high-frequency applications.

Table I. Quasistatic and dynamic parameters of $[Co_xFe_{100-x}$(20 Å)/oxide$]_{50}$ (see Ref. 7).

x (% Co)	H_k^{stat} (Oe)	H_k^{dyn} (Oe)	calc f_{FMR} (GHz)	meas f_p (GHz)	α
10	20	24(15)	2.0	2.1	0.016
30	49	51	2.8	3.0	0.012
50	88	88	3.5	3.7	0.014

MAGNETIC CHARACTERISTICS OF THE NATIVE OXIDE

Net Moment

The average net moment $\bar{\mu}_{net}$ of a MNOM is the sum of the net moments of the metal (μ_{net}^m) and oxide ($\bar{\mu}_{net}^{ox}$), weighted by their respective fractions, and may be written

$$\bar{\mu}_{net} = \bar{\mu}_{net}^{ox} + (\mu_{net}^m - \bar{\mu}_{net}^{ox}) f \ , \qquad (1)$$

where f is the atomic metal fraction. This relation provides a means to determine the constituent metal and oxide net moments through measurements of f and $\bar{\mu}_{net}$. As described in [8], a series

of Fe MNOM samples, $[Fe(t_0)/oxide]_N$, was prepared, with t_0 ranging from 5 Å to 60 Å. For each sample, f was determined from the fractional contribution of the metallic component to the area of its Mössbauer spectrum [8], and corresponded to the oxidation of a constant 8.4(2) Å of metal per layer irrespective of t_0. The fitting of the Mössbauer spectra was described in detail in [8], and will be summarized below. The net saturation moment of each MNOM was measured in a SQUID magnetometer. Fig. 3(a) shows the measured $\bar{\mu}_{net}$ versus f at 300 K for this series of samples. For $f > 0.4$ (or $t_0 > 14$ Å), $\bar{\mu}_{net}$ increases linearly with increasing f; as expected from (1) when μ_{net}^{m} and $\bar{\mu}_{net}^{ox}$ are constant. The slope and intercept of the fit of (1) to the data for $f > 0.40$ yields net moments of 2.1(1) μ_B/Fe and 1.38(6) μ_B/Fe for the metal and oxide, respectively. The metal moment is close to bulk α-Fe, 2.172 μ_B/Fe, while $\bar{\mu}_{net}^{ox}$ has a value close to that of magnetite (Fe_3O_4), 1.35 μ_B/Fe. A similar analysis at T = 5 K shows almost no temperature dependence in the data of Fig. 3(a): *μ_{net}^{m} and $\bar{\mu}_{net}^{ox}$ increase by only ~2% in cooling to 5 K*. This weak temperature dependence, similar to that of bulk α-Fe, indicates an oxide ordering temperature significantly higher than room temperature.

The large net moment of the buried native Fe oxide is preserved with the addition of at least 50% Co. Using f determined in [5] for the Fe and Co in $[Co_xFe_{100-x}(20 Å)/oxide]_{50}$ films for x = 30, 50, and 90, $\bar{\mu}_{net}^{ox}$ was determined from (1) by measuring $\bar{\mu}_{net}$ and assuming that the metal fraction takes its bulk moment for these compositions, as it does for x = 0. The variation of $\bar{\mu}_{net}^{ox}$ with alloy composition is summarized in Fig. 3(b). $\bar{\mu}_{net}^{ox}$ shows little change up to at least x = 50. However, in the Co-rich x = 90 MNOM, the oxide net moment is near zero. Importantly, the reduced $\bar{\mu}_{net}^{ox}$ at high Co fraction coincides with the loss of soft magnetic properties [Fig. 2(c)].

Oxide Magnetic Hyperfine Field Distributions and Magnetic Structure

Oxide Hyperfine Field Distribution: A room-temperature conversion electron Mössbauer (CEMS) spectrum for $[Fe(20 Å)/oxide]_{50}$ is shown in Fig. 4(a), and is typical of the spectra for t_0>14 Å. The splitting of a spectrum into six lines is due to a lifting of the nuclear spin degeneracy by the field of the atomic moment via the hyperfine field (HF) interaction. A relative shift along the velocity axis is termed the isomer shift (IS) and is related to the *s*-electron density at the nucleus. The IS thus provides a means to discriminate between metal (Fe^0) and oxide contributions to the spectrum. In Fig. 4(a) the metal and oxide subspectra are visible as two partially overlapping magnetically-split sextets, with the oxide shifted towards positive velocity relative to the metal.

Each CEMS spectrum was simultaneously fitted with metal and oxide sextets, fully described

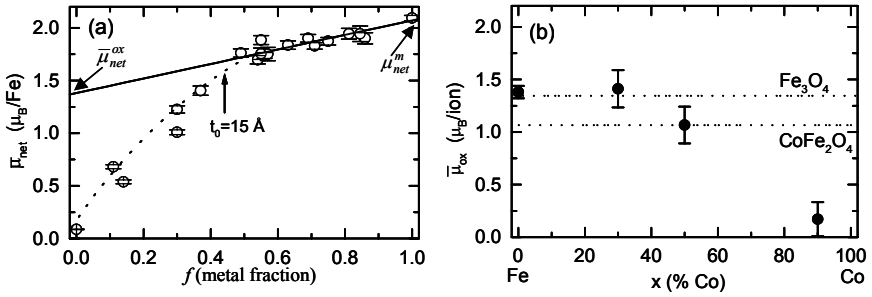

Fig. 3. (a) Room-temperature saturation moment versus metal fraction for a series of $[Fe(t_0)/oxide]_N$ of varying t_0. Solid line is a linear fit of the data for $f > 0.4$. Extrapolations to $f = 0$ and $f = 1$ give oxide and metal moments, respectively. (b) Room-temperature net moment of the native oxide for MNOMs of varying Co_xFe_{100-x} composition.

in [8]. The (fitted) HF and IS of the metallic component were close to those of bulk α-Fe [REF]. The oxide contributions to each spectrum were consistently fitted to a general hyperfine field distribution (HFD) model consisting of a discrete set of subspectra with equally-spaced HFs and variable relative areas. The HFD thus quantifies the fraction of oxide spins with a HF in a given range. In Fig. 4(b), the fitted Fe^0 subspectrum has been subtracted from the full spectrum in Fig. 4(a), revealing the oxide contribution. It consists of a relatively sharp magnetically-split sextet and a broad parabolic background, with the latter shifted towards positive velocity with respect to the former. The spectrum is fitted by the HFD of Fig. 4(c). The three dominant subspectra of the HFD, centered at 387 kOe and comprising 70(2)% of the oxide spectrum, fit the main oxide sextet, and have an average IS of 0.37 mm/s. The remaining lower-HF subspectra, with an average HF of ~140 kOe and IS of 0.65 mm/s, account for the broad, weakly-split component. We note that the HFs of this oxide stand are considerably lower than the bulk HFs of the moment-bearing Fe oxides (typically ~500 kOe).

Temperature Dependence and Implications: Applied fields up to 3 kOe have no significant effect on the oxide HFD, precluding oxide superparamagnetism as a source of HF reduction. However, *T*-dependent Mössbauer spectroscopy, presented in [8] for a t_0 = 20 Å Fe MNOM, revealed very different *T*-dependences in the HF splitting of the weakly and strongly-split oxide spectral components. With decreasing *T*, the main sextet showed little change, while the splitting of the broad component increased continuously. At 4.2 K, the broad component was replaced by a fully-split sextet, overlapping with and indistinguishable from the main sextet. This behavior suggests two *magnetic components* in the oxide. The "majority component", responsible for the weakly *T*-dependent main sextet, consists of ordered ionic sites stabilized by

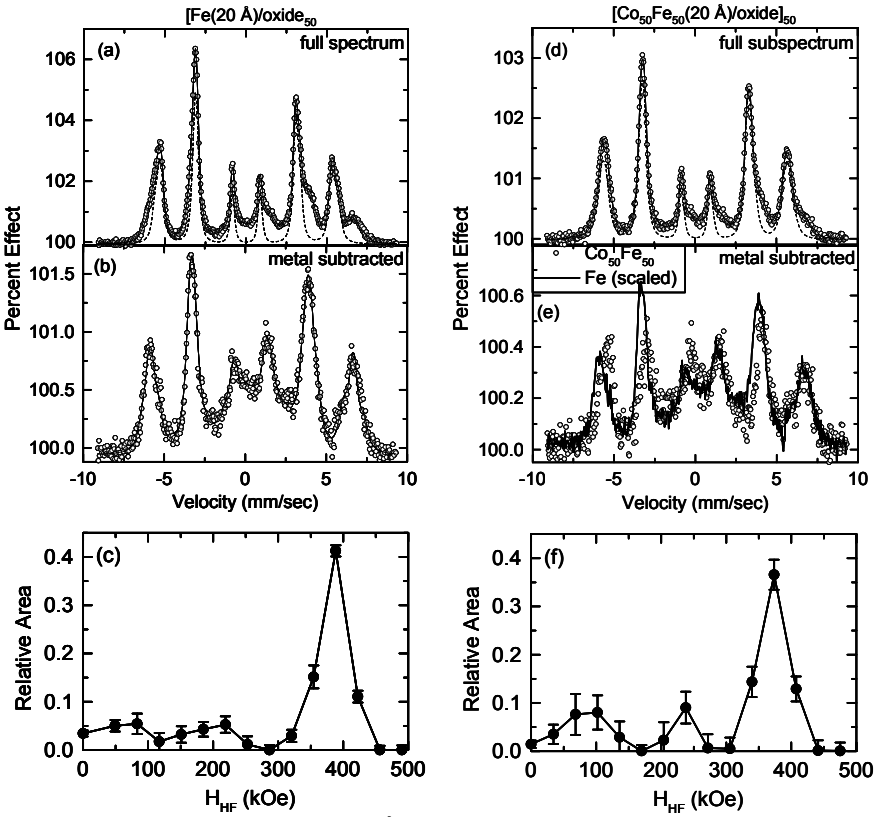

Fig. 4. (a) Room-temperature Mössbauer spectrum for $[Fe(20\ Å)/oxide]_{50}$, along with full fit (solid line) and metal subfit (dashed line). (b) Oxide subspectrum, obtained by subtracting metal fit from full spectrum in (a). Fitted oxide hyperfine field distribution is shown in (c). (d)-(f) Same as (a)-(c), but for $[Co_{50}Fe_{50}(20\ Å)/oxide]_{50}$. Oxide subspectra for the Fe and $Co_{50}Fe_{50}$ films are compared in (e).

a strong exchange field. The strong *T*-dependence and broad high-*T* distribution of the HFs of the remaining "minority component", suggest of ionic sites with a range of weak exchange fields.

The *T* dependence of the HF splitting follows that of the (local) ionic moment. The Mössbauer studies indicate that ~30% of the oxide spins have a strongly *T*-dependent ionic moment, with an average HF splitting that increases by a factor of ~4 from 296 K to 4.2 K [REF]. However, no significant change in the *net* moment accompanies this fourfold enhancement of the thermally-averaged *ionic* moment. *Thus, these spins must order such that their net moment is unaffected by a change in their average ionic moment; i.e., the spins must be arranged to yield no net moment.* Because the *minority component* spins bear no net moment, the measured $\overline{\mu}_{net}^{ox}$ of 1.37 μ_B/Fe [Fig. 3(a)], averaged over *all* the ions, arises only from the thermally-stable *majority component*, implying that the majority component spins contribute an average 2.0 μ_B/Fe to the net moment. The net moment of the majority component is much larger than the 1.15 μ_B/Fe and 1.37 μ_B/Fe found in γ-Fe_2O_3 and Fe_3O_4, respectively, and is comparable in magnitude and *T* dependence to that of α-Fe.

Fe versus CoFe: The room-temperature oxide CEMS subspectra (sensitive *only* to the Fe fraction) of a $[Co_{50}Fe_{50}(20\ Å)/oxide]_{50}$ MNOM is compared to the corresponding Fe MNOM in Fig. 4(d)-(f). EXAFS studies [5] indicate approximately equal oxidation of Fe and Co in this case, implying that ionic Co comprises ~half of the oxide. Remarkably, the incorporation of the Co has little effect on the local magnetism of the Fe, and in particular, the weakly-split minority and strongly-split majority oxide components are present in approximately the same proportion. In addition, the net moment of the $Co_{50}Fe_{50}$ native oxide is very close to that of the Fe native oxide, strongly suggesting that the Co ions also order with a considerable net moment.

Collapse of Oxide Magnetism

As $f \to 0$ (below $f \approx 0.4$), $\overline{\mu}_{net}$ drops precipitously to 0 [see Fig. 3(a)]. From (1) this evidently requires $\overline{\mu}_{net}^{ox} \to 0$ as $f \to 0$. The rapid reduction of the oxide net moment with decreasing *f* coincides with a collapse of its magnetic HF splitting. For *f* > 0.4, the (room-*T*) HFD is independent of *f*, but as $f \to 0$ below this threshold, the oxide component is increasingly

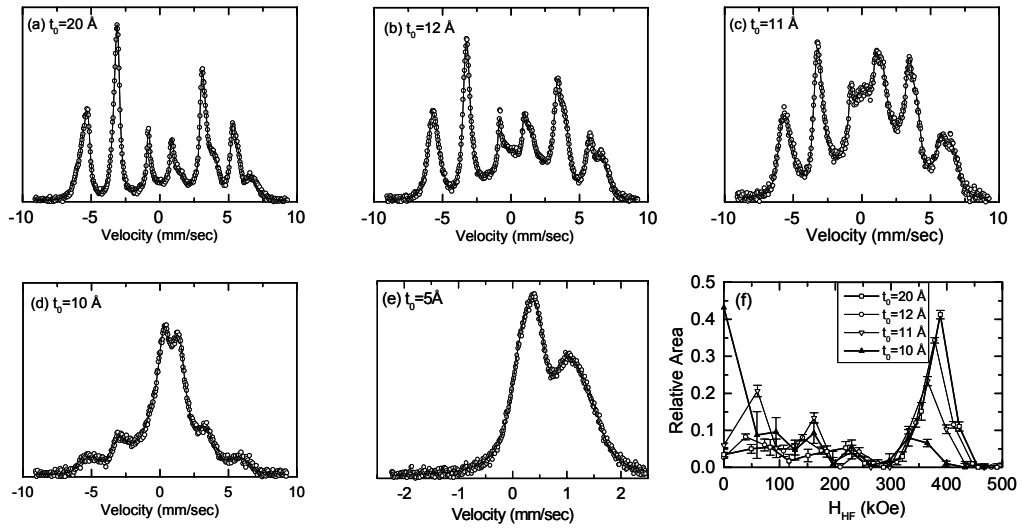

Fig. 5. (a)-(e) Room-temperature CEMS spectra (symbols) and fits (solid lines) for $[Fe(t_0)/oxide]_N$ films of varying t_0. (f) Corresponding hyperfine field distributions of the oxide component. Note the vanishing of spectral area near ~380 kOe between t_0=12 Å and t_0=10 Å.

dominated by weakly-split subspectra, seen in Fig. 5. In the limit of $f = 0$, realized for $t_0 = 5$ Å, the oxide CEMS spectrum is a nonmagnetic doublet characteristic of paramagnetic (nonstoichiometric) FeO. These data demonstrate a critical thickness $t_0^{crit} \approx 15$ Å above which the native oxide magnetic characteristics are invariant, but below which the oxide magnetism depends critically on the metal thickness. As ~8.4 Å of metal oxidizes irrespective of t_0, the collapse of the majority component in the HFDs of Fig. 5(f) between $t_0 = 12$ Å and $t_0 = 10$ Å corresponds to a nominal metal layer thickness dropping from ~3.6 Å to 1.6 Å. *The magnetism of the buried native oxide is stabilized by the proximate Fe metal and collapses in its absence.*

CONCLUSIONS

The Co_xFe_{100-x} MNOM system has a large magnetization and excellent soft magnetic properties including a low coercivity and a low-dispersion uniaxial anisotropy with a magnitude that is systematically tunable. The intrinsic resonance frequencies of these films extend to several GHz, making the MNOM an ideal candidate for high-frequency applications. The native oxide layers contribute significantly to the magnetization, and owing to their thickness, are strongly influenced by proximity with the metal.

ACKNOWLEDGEMENT

This work was supported in part by the National Institute of Standards and Technology's Nanotechnology Initiative. We acknowledge use of facilities at the Center for High Resolution Electron Microscopy at Arizona State University.

REFERENCES

[1] H. Fujimori, S. Mitani, S. Ohnuma, T. Ikeda, T. Shima, and T. Masumoto, "High electrical resistivity behaviour of Fe- and Co-based soft magnetic heterogeneous alloys," *Mater. Sci. Eng,* **A181/A182**, 897-901 (1994).

[2] M. Ohnuma, K. Hono, H. Onodera, S. Ohnuma, H. Fujimori, and J. S. Pedersen, "Microstructure and magnetic properties of Co-Al-O granular thin films," *J. Appl. Phys.,* **87**, 817-823 (2000).

[3] S. Ohnuma, N. Kobayashi, T. Masumoto, S. Mitani, and H. Fujimori, "Magnetostriction and soft magnetic properties of $(Co_{1-x}Fe_x)$-Al-O granular films with high electrical resistivity," J. Appl. Phys., **85**, 4574-4576 (1999).

[4] G. S. D. Beach, A. E. Berkowitz, F. T. Parker, and David J. Smith, "Magnetically-soft, high-moment, high resistivity thin films using discontinuous metal/native oxide multilayers," *Appl. Phys. Lett.*, **79**, 224-226 (2001).

[5] G. S. D. Beach, V. G. Harris, F. T. Parker, B. Ramadurai, David J. Smith, and A. E. Berkowitz, "Properties of the native oxide in metal/native oxide multilayers," *J. Appl. Phys.*, **91**, 7526-7528 (2002).

[8] G. S. D. Beach, F. T. Parker, David J. Smith, P. A. Crozier, and A. E. Berkowitz, "New magnetic order in buried native iron oxide layers," *Phys. Rev. Lett.*, **91**, 267201, (2003).

[7] G. S. D. Beach, T. J. Silva, F. T. Parker, and A. E. Berkowitz, "High-frequency characteristics of metal/native-oxide multilayers," *IEEE Trans. Magn.*, **35**, 2669-2671 (2003).

[8] G. S. D. Beach and A. E. Berkowitz, "Co_xFe_{100-x} metal/native oxide multilayers: a new direction in soft magnetic thin film design," submitted for publication (2004).

[9] T. J. Silva, C. S. Lee, T. M. Crawford, and C. T. Rogers, "Inductive measurement of ultrafast magnetization dynamics in thin-film Permalloy," *J. Appl. Phys.*, **85**, 7849-7862, (1999).